

Abstract

Absolute plate motion (APM) models derived from hotspot trails must satisfy trail geometries, ages and paleolatitudes, which requires modeling explicit plume motions. Models lacking plume motions or derived independently from seamounts must also fit that data, provided the implicit plume motions are geodynamically reasonable. We evaluate eight Pacific APM models; three have explicitly modelled plume motions. Seven derive from seamount age progressions; one is a geodynamic model driven by slab pull and ridge push. Using the long-lived Hawaii-Emperor and Louisville chains, we derive implicit motions of Hawaii and Louisville plumes for models lacking explicit estimates and compare them with observed paleolatitudes. Inferred plume motions are plausible given rheological constraints on mantle flow, but rates vary considerably and not all models fit data equally well. One potential endmember model predicts no APM direction change at 50 Ma, which best explains trails and paleolatitudes, minimizes predicted rotation of Pacific-Farallon ridge and assumes no true polar motion, yet its implicit plume drift is inconsistent with global circulation models. Alternatively, a global moving hotspot model yields acceptable fits to geometry and ages, implies a major APM change at 50 Ma, but requires significant true polar wander to explain observed paleolatitudes. The inherent inconsistency between age progressions and paleolatitudes may be reconciled by true polar wander, yet questions remain about the accuracy of age progressions for older sections of the Emperor and Louisville chains, the independent geologic evidence for an APM change at 50 Ma, and the uniqueness and relevance of true polar wander estimates.

1 Introduction

The plate tectonic revolution was quantified by determining the relative motions (RPM) between pairs of plates inferred from the pattern of magnetic lineations produced by seafloor spreading (McKenzie and Parker, 1967, Morgan, 1968, Le Pichon, 1968). However, it is also of interest to measure the absolute plate motion (APM) relative to the deep mantle, since such models are believed to more directly reflect the geodynamic forces acting on the plates. Seamount chains with approximately monotonic age progressions are believed to have formed over plumes in the mantle as the plate moved over them (Wilson, 1963). Changes in plate or plume motions would thus give rise to changes in the observed surface geometry of seamount trails. Traditionally, plumes were assumed to be fixed in the mantle or move very slowly relative to the motion of plates. With this assumption, a unique APM model can be determined. Thus, early in the plate tectonic revolution the $\sim 60^\circ$ Hawaii-Emperor Bend (HEB) was interpreted as primary evidence for an APM change (Morgan, 1971) estimated to have taken place ~ 42 Myr ago (Duncan and Clague, 1985); later age revisions have now placed the event closer to ~ 50 Myr (Sharp and Clague, 2006).

The Pacific plate is presently the largest of Earth's tectonic plates, representing seafloor from the present time back to the mid-Jurassic (e.g., Müller *et al.*, 2016). Given its longevity, it has recorded numerous events such as the formation and evolution of large igneous plateaus and several hotspot island and seamount trails. Unlike most other large tectonic plates, the Pacific carries no continents and is separated from those who do by destructive plate boundaries. It has therefore been difficult to determine its APM by propagating motions determined for other plates into the Pacific (e.g., Acton and Gordon, 1994, Raymond *et al.*, 2000). Most attempts to

81 independently establish a Pacific APM have relied on the Indo-Atlantic to Pacific plate circuit,
82 which involves Antarctica and Australia.

83 However, inferences of paleolatitude anomalies at several locations along such seamount
84 trails have been attributed to either true polar wander (Morgan, 1981; Gordon & Cape 1981;
85 Gordon 1983; Acton & Gordon, 1991; Petronotis et al. 1994) or motion of the hotspot (e.g.,
86 Tarduno and Cottrell, 1997, Tarduno et al., 2003), or a combination (e.g., Torsvik et al., 2017).
87 These anomalies seem to require that at least some, or perhaps all, of the hotspots have moved
88 significantly during the formation of the chains (Tarduno *et al.*, 2009). Given the width of
89 hotspot chains and the uncertainty in identifying current hotspot locations, any minor deviations
90 from rigid plates (e.g., Mishra and Gordon, 2016) can be ignored. Thus, the problem of
91 determining past APM reduces to finding the present and past locations of hotspots and the total
92 reconstruction rotations for a rigid plate at various times. While it is possible to come up with
93 models for such hotspot and plate motions, their uniqueness will depend on the data constraints
94 available. If no hotspot drift has taken place, then a best-fit solution can be derived from chain
95 geometry and age progressions alone (e.g., Duncan and Clague, 1985). However, if one or more
96 hotspots have moved over geologic time then the problem requires additional constraints. To
97 date, the only models that include hotspot motions have relied on mantle convection predictions
98 of plume behavior (Steinberger and O'Connell, 1998) or some idealized representation of hotspot
99 motion, based on such models (Steinberger and Gaina, 2007). Such flow models strongly depend
100 on rheological parameters and the history of past plate motions, as well as assumptions about the
101 mantle's heterogeneous density structure at past times. By selecting flow calculations whose
102 predictions of plume motion generally satisfy the limited paleolatitude data, one can combine
103 these hotspot location predictions with chain geometry and age data to solve for the complete
104 APM model (e.g., Doubrovine *et al.*, 2012, O'Neill *et al.*, 2005, Steinberger *et al.*, 2004;
105 Steinberger, 2000). The scarcity of paleolatitude data and the nonuniqueness of flow model
106 predictions have yielded a variety of APM models whose trail predictions approximately follow
107 the observed trails. Given the large number of additional parameters involved in modeling
108 moving hotspots, it is not clear that these models describe the motions of plates well or if they
109 are geodynamically feasible, especially given their approximate fit to data. For instance, plume
110 drift predictions (Doubrovine et al., 2012) for the last 5 Ma have been shown to be at odds with
111 recent motions inferred from observations (Wang et al., 2019), suggesting that more data need to
112 be included in order to constrain such models.

113 Torsvik *et al.* (2017) suggested that the implied plume and plate motions required to explain
114 the HEB entirely in terms of southward plume motion, as Tarduno *et al.* (2009) has argued, are
115 simply not compatible with the motions predicted by mantle circulation models and the relative
116 plate motion history of the Pacific. Consequently, they argued that a prominent change in APM
117 must be required to explain the observed geometry and age progression. Reigniting the debate
118 over which geodynamic forces could have driven the Pacific plate northward before the HEB,
119 Domeier *et al.* (2017) suggested that an east-west oriented intraoceanic subduction zone to the
120 north may provide the missing piece. These interpretations have implications for how the
121 paleolatitudes obtained from the Emperor seamounts should be interpreted, with perhaps a
122 considerable amount needing to be attributed to true polar wander (TPW, Morgan, 1981, Gordon
123 and Cape, 1981, Petronotis et al., 1994, Koivisto *et al.*, 2014; Woodworth and Gordon, 2018). In
124 strong contrast to these views are the arguments recently made by Bono *et al.* (2019) which
125 reiterate that the HEB was caused by southward plume motion and that true polar wander can be
126 excluded as a relevant factor. The range of published arguments would therefore seem to suggest

127 that the motion of the Pacific plate and the plumes beneath it remains an unresolved problem in
128 plate tectonics.

129 Here we investigate eight published APM models, representing a mix of fixed and moving
130 hotspot assumptions. The purpose of this paper is to examine the amount of hotspot motion
131 implied by each model, measure the extent to which the models fit the available data and are
132 geodynamically reasonable, and examine if the hotspot motions are realistic given constraints on
133 rheology of the upper mantle.

134

135 **2 Data**

136

137 We focus our attention on just the Hawaii-Emperor and Louisville hotspots and trails since
138 their longevity means they dominate the information on Pacific plate motion for ages older than
139 30 Ma. While new data are now available to support a similar longevity for the Rurutu hotspot
140 (Konrad *et al.*, 2018), unlike for Hawaii and Louisville there are no paleolatitude constraints to
141 consider. Fig. 1 presents the geometric, chronologic, and paleomagnetic data available for the
142 older sections of these two seamount chains (Tarduno, Duncan *et al.* 2003, Clouard and
143 Bonneville 2005, Kono, 1980, Koppers, Gowen *et al.* 2011, Koppers, Yamazaki *et al.* 2012,
144 Bono, Tarduno *et al.* 2019). Following Wessel and Kroenke (2009), we have determined an
145 empirical median line for each seamount trail and used these spatial curves to derive continuous
146 and smooth age progression curves using splines (Fig. 2). Similar analyses were also performed
147 by O'Connor *et al.* (2013), Doubrovine *et al.* (2012) and Konrad *et al.* (2018). There are several
148 points to note from these age progressions: (1) the data scatter about the mean trend (generally in
149 the $\pm 2\text{--}4$ Myr range) greatly exceeds the individual age uncertainties, (2) considerable smoothing
150 is necessary to avoid age reversals along track, (3) despite much recent sampling (e.g., Koppers
151 *et al.*, 2011, Koppers *et al.*, 2012, O'Connor *et al.*, 2013), the two chains feature several sections
152 where age progressions are poorly expressed, and (4) the age of the respective bends in the trails
153 are statistically indistinguishable from Chron 21o (47.9 Ma), yet the large number of age
154 determinations at these bends exhibit a wide range of values. While our spatial curves are
155 subjective, experiments with different median lines show the above conclusions are robust. The
156 methodology can nevertheless be improved further.

157 Much work has been done to understand the APM of the Pacific plate and the plumes over
158 which it has moved (e.g., Doubrovine *et al.*, 2012, Duncan and Clague, 1985, Koppers *et al.*,
159 2001, Wessel and Kroenke, 2008, Wessel and Kroenke, 2009, Steinberger *et al.*, 2004). The most
160 critical region for such studies involves the Emperor and the coeval old section of the Louisville
161 chain. Fig. 2 shows that serious data gaps continue to hamper a detailed understanding of these
162 chains. For instance, for a length of ~ 1200 km north of the Louisville bend (LVB) we find sparse
163 ages with variability far beyond the apparent smoothness of the age progression model. In fact,
164 here our smooth model is poorly supported by the data, with individual misfits exceeding 4–6
165 Myr. The situation for the Emperor chain is not much better. We find an 800-km gap in dated
166 samples between Suiko and Detroit seamounts, while further south we have a 400-km section
167 with three samples that all suggest an approximate seamount age of ~ 55.5 Ma. When our two age
168 progression curves are used to derive the inter-hotspot separations (Wessel and Kroenke, 2009),
169 the 400 km section of near-constant age translates to a large 3.4° offset in separation distance that
170 divides two periods of approximately stable plume distances. It seems unrealistic to invoke
171 extremely rapid plume or plate motions to explain the apparent constant ages, suggesting instead
172 that the age data are not representative of the actual age progression along the Emperors.

173 Alternatively, we are likely seeing the back-and-forth surface manifestation of the nonlinear
174 dynamics of a thermochemical plume (Ballmer *et al.*, 2013). Clearly, more and denser data will
175 be required to resolve this dilemma. For now, we will employ the two smooth, continuous and
176 monotonic age progression curves (Fig. 2) as representative of the variation in age along the two
177 trails, despite any shortcomings in data quality.
178

179 **3 Methods**

180
181 We examine a representative subset of published APM models that reflects a range of
182 model behaviors, including the two fixed Pacific hot spot models KMM01 (Koppers *et al.*, 2001)
183 and WK08A (Wessel and Kroenke, 2008). These two models have a similar origin as they are
184 only constrained by Pacific seamount track geometries and age progressions and do not consider
185 paleolatitudes or hotspot motions. We include a partially fixed hotspot model (WK08D) in which
186 the Hawaii hotspot implicitly migrates south during the Emperor stage at a rate selected to
187 produce no change in plate motion direction (Chandler *et al.*, 2012). It thus shares the
188 assumptions of the three fixed APM models except during the Emperor stage. Next, we include
189 two moving (OMS05, O'Neill *et al.*, 2005, H2016, Hassan *et al.*, 2016) and one fixed (M2015C,
190 Maher *et al.*, 2015) hotspot model satisfying data from the Indo-Atlantic realm and projected into
191 the Pacific via the Africa–India–East Antarctica–Mary Byrd Land–Pacific plate circuit. Thus,
192 these three models were derived from similar seamount trail data from the Indo-Atlantic but
193 differ in that OMS05 used a moving hotspot reference frame tied to Africa while H2016 used the
194 Torsvik *et al.* (2008) hybrid reference frame; the H2016 model also used a modified set of
195 relative plate rotations to derive a Pacific APM model. We also include a global moving hot spot
196 model (D2012) fitting five major hot spot chains from three of the world's major ocean basins
197 (Dobrovine *et al.*, 2012). This last model therefore is constrained by global seamount tracks as
198 well as hotspot drifts largely consistent with observed paleolatitudes. Finally, we considered an
199 APM model (B2014) predicted by geodynamic modeling of slab pull and ridge push
200 (Butterworth *et al.*, 2014). Unlike most other APM models (but see Gordon *et al.*, 1978 for a
201 similar approach), this model is independent of seamount geometry and age-progressions and is
202 only constrained by geodynamic boundary forces. The B2014 model only portrays Pacific APM
203 during the 72–42 Ma time interval and thus was augmented with rotations from the most similar
204 APM model (WK08D) for the more recent motion since 42 Ma; we also extended B2014's
205 oldest stage rotation back to 80 Ma.

206 While there are additional moving hotspot APM models discussed in the literature (e.g.,
207 Koppers, Duncan *et al.* 2004, Steinberger, Sutherland *et al.* 2004, Torsvik, Müller *et al.* 2008),
208 they are not easily reproducible because the coordinates of plume paths were not published along
209 with the plate rotation parameters. Based on these eight APM models, Fig. 3 shows the past
210 motion of the Pacific plate predicted for points that originated at the (present) Hawaii (HI) and
211 Louisville (LV) hotspots. The colored tracks thus reflect APM and should only honor the two
212 seamount trails if the APM model assumed no hotspot motion; this includes KMM01 and WK08
213 for the Pacific and M2015C from the Indo-Atlantic domain. This is so because in that scenario
214 the trails are assumed to reflect the entire APM whereas for the moving hotspot models at least
215 part of the geometry will be attributed to the motion of the plumes. Consequently, the past
216 motions of a point beneath the present hotspots and the corresponding trail geometries depart,
217 reflecting various amounts of hotspot motion.

218 Given a model for Pacific APM we can now take the continuous age-progression curves (Fig.
219 2) and reconstruct each point along the curves back to zero age. This technique was

220 independently developed by Torsvik *et al.* (2017) and Wessel and Conrad (2017). For models
221 derived for fixed hotspots these reconstructions should all fall close to the present (fixed) hotspot,
222 while for models designed relative to a set of moving hotspots the reconstructions should reflect
223 the prescribed plume paths. Finally, for models determined for other ocean basins but propagated
224 into the Pacific via a plate circuit the reconstructions will show the plume motion history that is
225 required for the APM model to satisfy the age-progression constraints from Pacific seamount
226 trails alone. In other words, given observed age-progressions and an APM we can extract the
227 *implicit* plume drift histories for each trail. We have made these calculations for the eight
228 published APM models listed above and present them separately for Hawaii (Fig 4a) and
229 Louisville (Fig. 5). In addition to reconstructing the inferred hotspot motion paths we also
230 reconstructed individual age samples as colored triangles (and these will scatter about the
231 reconstructed plume paths since the latter is a smooth continuous representation of the former) as
232 well as the limited paleolatitude estimates (circles) from each trail (Koppers *et al.*, 2012,
233 Tarduno *et al.*, 2009; Bono *et al.*, 2019). The colors of these circles reflect the misfit between
234 observed and predicted paleolatitudes; see color scale in Fig. 4 for range.

235

236 **4 Results**

237

238 Examining the plots in Figs. 4 and 5, we see similar responses for the two fixed hotspot
239 models KMM01 and WK08A for HI (Fig. 4). Since these two APMs were designed relative to
240 fixed hotspots, the reconstruction of the hotspot paths should ideally converge on a single point,
241 i.e., the fixed hotspot. This is generally true, at least for the younger sections, and some of the
242 discrepancies relate to revised age progressions since the models were published. For ages
243 younger than 55 Ma the reconstructions are compatible with a single point (i.e., we observe
244 modest scatter around the present hotspot consistent with the scatter in Fig. 2). However, for
245 older ages both models diverge. The KMM01 model requires a $\sim 5^\circ$ north to south motion for the
246 same time frame. The WK08A model fails to fit the oldest Hawaii and Louisville trail as well
247 and requires a correction in the form of a north then south plume motion due to systematic
248 misfits to the age progressions. In addition, both models fail (by design) to explain the
249 paleolatitudes. Examining the predictions for LV for the same two models (Fig. 5), we notice
250 much larger discrepancies. KMM01 struggles to fit the age-progression, which has been revised
251 by several new data sets collected after KMM01 was first developed. In contrast, WK08A
252 benefitted from some of the newer LV age data and shows less scatter, yet several degrees of
253 ESE to WNW plume motion is implied for the older Louisville section. As for the Hawaii-
254 Emperor chain, both models fail to satisfy the LV paleolatitude constraints by reconstructing the
255 locations too far south.

256 The next APM candidate (WK08D) is a hybrid model that originated as a fixed hotspot model
257 from the present back to the HEB (i.e., WK08A), but then the rotations for the Emperor age
258 interval were adjusted to fit only the Louisville trend while simultaneously ignoring the
259 geometry of the Emperor track to yield no change in APM direction at HEB. While no moving
260 hotspots were explicitly used to derive these rotations, the steady westward motion predicted by
261 the model implicitly requires the HI plume to have moved south during the Emperor formation.
262 Fig. 4 reflects the implied nature of this required plume motion. For times before the HEB
263 formation the plume is required to have moved westward then southwest to its present location.
264 This plume history comes closer to fitting the paleolatitudes but underperforms for the oldest
265 samples. Because the APM model still fits the Louisville chain, the plume predictions there (Fig.

266 5) are similar to WK08A and hence fail to address the paleolatitude anomalies (which were
267 obtained after WK08D was published).

268 The OMS05 model is an Africa plate-based model defined relative to a set of moving Indo-
269 Atlantic plumes (O'Neill *et al.*, 2005), and we have projected the finite rotations into the Pacific
270 via the Africa–India–East Antarctica–Mary Bird Land–Pacific plate circuit; other plate circuits
271 are of course also possible but for consistency we use this one when projecting Indo-Atlantic
272 models into Pacific. As such, there is no model drift for Pacific plumes to which we can compare
273 our results. When reconstructing the age-progressions using this model we obtain the implicit HI
274 and LV plume motions required to match the age and geometry observations. For HI, the
275 OMS05 implies a near-sinusoidal plume drift with its most distal latitude reached around 60 Ma
276 and then returning south for older ages. Thus, some paleolatitudes are adequately explained but
277 the oldest observations are not. The situation for LV is similar, i.e., a large excursion of implied
278 plume drift with modest predictive powers to explain observed paleolatitudes. The H2016 model
279 was developed to support the claim that a rapid burst of hotspot motion is needed to explain the
280 formation of the HEB (Hassan *et al.*, 2016). However, while the combination of their modelled
281 plume motion and Pacific APM approximately predicts the Hawaii-Emperor trail, the age
282 progressions are not well matched, resulting in an implicit plume drift quite different from their
283 explicit path (Fig. 4). For Louisville the model does not match the geometry and age progression
284 very well (Fig. 3), and the implicit drift curve is very different from that modelled (Fig. 5). Part
285 of the explanation of the misfit is likely related to the fact that the model Louisville plume
286 emanated very far from the actual Louisville location, and while the predictions were translated
287 the mantle flow regimes at the two sites are unlikely to be similar (Hassan, pers. Comm., 2018).

288 When examining predictions from the fixed Africa hotspot model M2015C (Maher *et al.*,
289 2015) we surprisingly find a very similar situation in that the inferred hotspot motions in the
290 Pacific to first order equal those of other Indo-Atlantic models. This similarity suggests that the
291 main cause of the implied plume motions may have its origin in the plate circuit, which possibly
292 may be inaccurate for older ages (e.g., Acton and Gordon, 1994, Koivisto *et al.*, 2014), but
293 relative plume drift between Atlantic and Pacific hotspots may also play a role.

294 The next APM candidate (D2012) is the only model that describes global APM relative to five
295 long-lived plumes distributed across three ocean basins (Dobrovine *et al.*, 2012). Both the HI
296 and LV plumes were among the plumes modeled and their expected motions were included when
297 fitting the APM (and displayed in Fig. 3). In the case of HI, we find that the plume is relatively
298 stationary back to ~55 Ma, but earlier there is an almost north to south drift. While this motion
299 helps to reduce the paleolatitude anomalies, it is still failing to explain their full range, especially
300 for the oldest Emperor section. For LV, there is more east-west motion implied, and as for HI the
301 paleolatitudes are under-predicted. The overall shapes of the implicit plume motions (from
302 smoothed age progressions) to first order match the prescribed (explicit) plume motions for this
303 model (Fig. 3; also shown for this panel in Fig. 4), yet the explicit and implicit D2012 plume
304 motions have significant differences, particularly in longitude.

305 Our final model (B2014) differs from all other APM models as it is a geodynamic model
306 driven by forces acting on the Pacific plate (Butterworth *et al.*, 2014). Hence, no seamount trail
307 geometry and age progressions were used, and it may therefore serve as an independent test of
308 expected Pacific motion driven by boundary forces. For HI, this APM model implies a strong
309 monotonic plume drift from NNE to SSW over the timeframe ~80 Ma to ~50 Ma, and
310 consequently the plume history largely matches the paleolatitude constraints. The situation is
311 very similar for LV, where an almost north-to-south plume motion during the same timeframe is

312 implied. As for HI, the LV paleolatitudes are well modelled. However, B2014 is not
313 representative of all geodynamic models being driven by boundary forces. Earlier efforts (e.g.,
314 Gordon et al., 1978, Conrad and Lithgow-Bertelloni, 2004, Faccenna et al., 2012) also
315 considered different combinations of forces acting on the base and/or edges of the Pacific plate,
316 but their results diverge from B2014, especially for the Emperor era due to different plate
317 geometries and different forcing combinations. Further evaluations of such models may address
318 the uniqueness of geodynamic APM models and their dependence on past plate tectonic histories.
319

320 **5 Discussion**

321
322 Clearly, the APM models examined differ in the amount and direction of predicted or implied
323 plume drift. The fixed hotspot models highlight the long-known fact that most of the observed
324 Pacific age progressions can be fit with a fixed hotspot model, but this condition breaks down
325 around 55–60 Ma (Wessel and Kroenke, 2009, O'Connor *et al.*, 2013). Furthermore, they ignore
326 the observed paleolatitudes, instead (implicitly) attributing the paleolatitude anomalies to TPW
327 (e.g., Wessel and Kroenke, 2008), which would seem to be in the 5–10° range (Torsvik *et al.*,
328 2017). That some of the mismatch between observed and predicted paleolatitudes may be due to
329 TPW is not a new idea (e.g., Morgan, 1981, Gordon and Cape, 1981, Petronotis et al, 1994), and
330 some authors consider TPW to have played a much larger role during the formation of the HEB
331 (e.g., Woodworth *et al.*, 2017, Wilson, 2016). It is also possible that uncertainties in the global
332 plate circuit prevent accurate predictions of Indo-Atlantic models projected into the Pacific (e.g.,
333 Koivisto *et al.*, 2014, Acton and Gordon, 1994).

334 One key distinguishing feature of the predictions in Fig. 4 is the difference between the
335 Pacific models and the Indo-Atlantic models projected into the Pacific. Despite the differences
336 between the OMS05 (moving Indo-Atlantic plumes) and M2015C (fixed hotspots) models, both
337 yield to first order very similar plume predictions for both HI and LV (again, specifics depend on
338 the plate circuits). Part of this is expected, since the modelled plume motions in OMS05 for the
339 post-80 Ma period are statistically insignificant (O'Neill *et al.*, 2005). We interpret the first-order
340 NE-to-SW drift pattern to reflect either artifacts in the plate circuit or systematic differences
341 between Pacific and Indo-Atlantic plume drifts.

342 A recently proposed technique called “ridge-spotting” has been used to test the validity of
343 APM models (Wessel and Müller, 2016). Ridge-spotting combines both APM and RPM and
344 explores model predictions for the long-term behavior of spreading ridges. While all tested APM
345 models predicted large amounts of northward migration and monotonic clockwise rotation of the
346 Pacific-Farallon ridge, it was not immediately clear if the technique ruled any APM model out.
347 However, it seemed intuitive that models predicting large-scale ridge rotation were
348 geodynamically the least likely. Furthermore, the Africa-based models resulted in extensive east-
349 to-west ridge migration that more likely reflects inaccuracies in the plate circuit than actual ridge
350 dynamics. The B2014 model was considered to be the most stable model in that it predicted the
351 smallest amount of ridge rotation (Wessel and Müller, 2016). Yet, we caution that minimal
352 implied ridge rotation may not necessarily be a defining characteristic of an optimal APM model,
353 but also note that Becker *et al.* (2015) in fact suggested a “ridge-no-rotation” reference frame as
354 a possible candidate for APM. The B2014 model predictions are further highlighted in Fig. 6
355 where we take the implied plume motions for HI and LV and use them with the B2014 rotations
356 to predict the HI and LV seamount trails. While the generally good fit to the observed seamount
357 ages is partly a consequence of the way we reconstruct the implicit plume paths, the straightness

358 of the plume paths and the good fit to observed paleolatitudes is what distinguishes B2014 from
359 all other APM model predictions in Fig. 4. Unlike D2012, the B2014 model predictions for
360 Louisville shows straight and extensive north-to-south drift, thus matching the Louisville
361 paleolatitudes better than other models. We do note the D2012 rotations appear to contain
362 components that yield a systematic offset along the oldest section of the Emperor trail (Fig. 6).
363 Hence, there may be important discrepancies between D2012's geodynamic predictions and
364 actual Pacific plate motions for the pre-60 Ma period, notwithstanding the broader scope of
365 D2012 (global) versus B2014 (Pacific only).

366 If we examine the plume drift rates that are implied by the APM models and the observed
367 age progressions, we find that plume drift predictions vary considerably and, in some cases, have
368 large differences before and after HEB time. Fig. 7 shows the mean pre/post-HEB predictions for
369 both the (a) Hawaii and (b) Louisville plumes. The drift rates were obtained by taking the
370 predicted plume paths histories and estimating a time derivative via finite differences. Because
371 discrete APM models may yield jumps in speeds and since the noise in the empirical age
372 progressions will be amplified by the finite differencing, we have averaged the results for either
373 side of the HEB. There are several observations we can make from these results: (1) There is
374 broad agreement that plume drift rates following the HEB event are in the 1.5–2.5 cm/yr for
375 Hawaii and 0.5–1.5 cm/yr for Louisville. All models, whether explicitly modeling drift or not,
376 have explicit or implicit rates in these ranges. (2) The pre-HEB domain presents a dramatically
377 different picture, with a wide range of average drift rates from 2–7 cm/year. Implicit plume
378 motions for the two Africa-derived models are both very high, regardless of being a fixed or
379 moving Africa hotspot model. The geodynamic B2014 model shows a 6 cm/year average rate
380 required to fit the seamount geometry. The Pacific fixed hotspot models show little change, as
381 discussed earlier – their main failing lies in ignoring paleolatitudes. The H2016 model explicit
382 drift rate for Hawaii is considerably higher than that of the D2012 explicit rates, by a factor of
383 two. (3) All implicit mean plume drifts exceed observational speed limits for the post-HEB era
384 (Koivisto et al., 2014) as well as inferred hotspot drift rates for the last ~5 Myr (Wang et al.,
385 2019).

386 Despite the conclusions of Tarduno *et al.* (2009) and Bono *et al.* (2019) suggesting the HEB
387 predominantly reflects a change in north-to-south plume motion, there has been evidence
388 presented in the literature that appears to require a significant component of plate motion change
389 (Wessel and Kroenke, 2009, Woodworth *et al.*, 2017). Recently, Torsvik *et al.* (2017)
390 demonstrated that a Pacific APM change at HEB time is in fact required by showing predictions
391 of three simple plume/plate motion scenarios (their Fig. 3). In all three cases the Pacific plate
392 motion undergoes no change in direction. The first two cases maintain a constant Pacific angular
393 velocity throughout and highlight the directions and rates of plume motions required to satisfy
394 the Emperor geometry. In case 1, to satisfy Emperor age progression a plume drift of $0.6^\circ/\text{Ma}$
395 (6.7 cm/yr) from the NW is required, but there is no geodynamic basis for the plume to drift in
396 this direction (Torsvik *et al.*, 2017). In contrast (case 2), a more north-to-south drifting plume
397 (which is much closer to actual predictions from mantle circulation models) would need an
398 excessive drift rate of $3.8^\circ/\text{Ma}$ (42 cm/yr) to match the geometry, yet at this rate it grossly fails to
399 match the observed Emperor age progression. Finally, they show (case 3) that a north-to-south
400 drifting plume at $0.58^\circ/\text{Ma}$ (6.4 cm/yr) rate can fit both geometry and age progression, provided
401 the Pacific APM motion was vastly slower prior to the HEB. Seen in this context, B2014 may
402 represent a blend of their first and third cases: A drift direction (from $\text{N}33^\circ\text{E}$) closer to SSW than
403 S, but with a drift rate closer to $0.5^\circ/\text{Ma}$ (5.6 cm/yr). Interestingly, the APM models unaffected

404 by Pacific hotspot trails (OMS05 and M2015C) have implicit plume motions that, to first order,
405 have key similarities with those of B2014: a plume trail trending from an azimuth of $\sim 30^\circ$ (Fig.
406 4). While this could be a coincidence related to systematic uncertainties in the plate circuit, it
407 could also be taken as supporting evidence for a component of SW drift prior to the HEB,
408 consistent the above-described case 1. Furthermore, the B2014 model shows that slow motion of
409 the Pacific plate prior to the HEB, as required by the above-described case 3, is consistent with
410 the time-evolution of forces on that plate. On the other hand, the need for Hawaiian plume drift
411 to the SW or SSW is not consistent with models of mantle flow, which indicate drift to the S or
412 SSE without a westward component (e.g., Torsvik *et al.*, 2017).

413 As for the plate speed change required in case 3, Fig. 8 shows the predicted plate motion
414 speeds at Hawaii and Louisville for the models discussed. We note the predictions of B2014 are
415 in the same sense as suggested by Torsvik *et al.* (2017) (the plate was moving slower prior to the
416 HEB), yet the change is closer to a factor of 2 than their factor of 6 because B2014 also includes
417 a compensating component of westerly plume drift (as in Torsvik *et al.*'s [2017] case 1).
418 Isochrons from the seafloor between the Clarion-Clipperton fracture zones covering the HEB
419 transition indeed show a corresponding sharp increase in RPM after the HEB (Barckhausen *et al.*,
420 2013), which likely reflects an increase in APM. This behavior strengthens the idea that some
421 aspects of B2014 may be valid but further refinements may be needed. Interestingly, while the
422 B2014 is obviously a geodynamical model driven by boundary forces, its prediction of Hawaii
423 plume motion has too much east-to-west motion (i.e., case 1) compared with other predictions
424 from mantle circulation models (e.g., Doubrovine *et al.*, 2012, Steinberger, 2000, Steinberger *et*
425 *al.*, 2004). For the recent geological past, these models predict plate speeds that are largely
426 compatible with estimates obtained by inverting current hotspot trail trends and the MORVEL
427 model (Wang *et al.*, 2019). Yet, there are some large excursions predicted by the WK08 models
428 that are likely the result of overemphasizing the age progression changes seen in the Hawaiian
429 Islands (e.g., Clague, 1996).

430 The two models with explicit plume drift predictions (D2012 and H2016) are further
431 compared with B2014 by examining longitude and latitude separately versus time (Fig. 9). This
432 analysis makes it clearer that the implicit plume drift for D2012 largely matches its explicit drift
433 as far as latitude is concerned, but has larger and systematic discrepancies in longitude,
434 especially for Hawaii. In contrast, the H2016 implicit and explicit curves show more variability
435 and larger discrepancies, especially in longitude. These discrepancies are largest for Louisville,
436 which we attribute to their plume being modelled too far from the actual Louisville location. Fig.
437 9 makes it clear that B2014 best satisfies the paleolatitude data, in particular for the oldest and
438 largest anomalies, provided that TWP is insignificant.

439 A final way to compare and contrast the APM predictions is to examine the paleolatitude
440 misfits (seen in Figs. 4 and 5) with respect to the change in plume drift across the HEB. Fig. 10
441 shows this data set for all models and it makes it clear that models trade off what they wish to
442 minimize (whether implicitly or explicitly). Models that we know provide very good fits to the
443 paleolatitude anomalies require a large change in drift rate before/after the HEB (e.g., B2014),
444 while models with a steady drift rate have significantly poorer fits to the paleolatitudes (e.g.,
445 most models, including D2012). However, as Torsvik *et al.* (2017) point out, this relationship
446 can change completely if TPW is used to adjust the paleolatitudes. Establishing robust estimates
447 for TPW with broad community acceptance would be an important contribution that has the
448 potential to settle the debate of the origin of the Hawaii-Emperor Bend.

449

450 **Conclusions**

451
452 D2012 and B2014 represent two different compromises of moving hotspot APM models for
453 the Pacific: On one hand, the B2014 model fully attributes both the HEB and LVB to plume drift,
454 predicts no APM change in direction, and maximizes the fit to observed paleolatitudes by
455 assuming no TPW. At the same time, it yields a very good fit to the geometry and age
456 progressions and is based on geodynamic estimates of plate-driving forces. However, B2014 also
457 requires a factor of 2.5 speedup of Pacific plate motions (Fig. 10) and a factor of 3 slowdown of
458 plume drift (Fig. 7) at HEB time. Also, like all geodynamic models, B2014 is dependent on
459 assumptions about plate forces and mantle rheology, and is therefore nonunique. On the other
460 hand, D2012 allows for a significant change in the direction of Pacific plate motion (Fig. 3), and
461 therefore does not require large changes in plume drift rate (Fig. 7) or plate speed (Fig. 10).
462 However, D2012 fits the geometry and age progressions less well (trail predictions deviate
463 systematically for older ages Fig. 6) and requires considerable TPW adjustment to explain the
464 large paleolatitude anomalies (Fig. 10).

465 While D2012 attributes the HEB/LVB to a change in the direction of Pacific plate motion,
466 B2014 requires plume drift rates to slow by a factor of ~ 3 during the HEB/LVB (Fig. 7). Such
467 rapid changes to the motions of both plates and plumes are challenging to explain
468 geodynamically (e.g., Richards and Lithgow-Bertelloni, 1996) because both are driven by mantle
469 buoyancy forces that change only gradually with time. However, plate motions are sensitive to
470 rheological processes such as plate fracture or strain-localization that can change plate-driving
471 forces rapidly with time (e.g., Bercovici *et al.*, 2000), for example via slab cessation or breakoff,
472 or plate boundary formation. By contrast, plume motions are sensitive to a vertically-integrated
473 column of slowly-moving mantle (Steinberger *et al.*, 2004), which should make rapid changes in
474 drift rate difficult. However, Tarduno *et al.* (2009) proposed that capture of the Hawaiian plume
475 by the Kula-Pacific ridge may have relaxed at about 80 Ma, resulting in southward plume drift
476 toward the current position of Hawaii by about 50 Ma (although we note this runs counter to the
477 conclusions of Petronotis *et al.*, 1994). This might make the B2014 plume drift scenario feasible
478 for Hawaii (Fig. 4), but cannot explain the similar slowdown of Louisville plume drift (Fig. 5)
479 because there is no ridge north of Louisville to capture that plume. These arguments seem to
480 favor models such as D2012 that explain both the HEB and LVB via a change in direction of the
481 Pacific plate, which is common to both plumes. Otherwise, a broad change in mantle flow
482 patterns beneath the entire Pacific (e.g., induced by a major change in plate motions or descent of
483 a new slab into the lower mantle) is required to simultaneously change the drift rates of both
484 plumes.

485 One possible explanation for the conflict between the B2014 predictions and the
486 requirements of plume behavior as proposed by Torsvik *et al.* (2017) may lie in an incomplete
487 description of the boundary forces acting on the Pacific plate. The realization that the Emperor
488 chain may after all reflect a more northerly motion of the large Pacific plate before HEB time has
489 resurrected the suggestion (Gordon *et al.*, 1978) of a missing east-west oriented subduction zone
490 to the north (Domeier *et al.*, 2017). While this suggestion remains speculative, if substantiated it
491 would indeed provide a geodynamic scenario where northward Pacific plate motion would be
492 predicted, reducing the magnitude of plume drift required to match seamount trail geometry and
493 age progressions. A corollary of this interpretation would be that D2012 may represent the best
494 model to date, despite implying a much higher Pacific-Farallon Ridge rotation than B2014 and
495 being more dependent on TPW to satisfy observed paleolatitudes. It unequivocally requires a

496 change in APM motion to explain the HEB and Emperor alignment (which is extended due to
497 plume drift). The largest caveat in our analysis of plume motions comes from the level of
498 uncertainty expressed in Fig. 2. It is possible that further age determinations along the poorly
499 dated sections could alter the final age progressions and hence drift rates. Hence, the balance
500 between plate and plume motions in the Pacific remain poorly quantified but could be further
501 clarified with improved age dating along the older sections of both the Emperor and Louisville
502 seamount chains.

503 Finally, we note that while geodynamic models such as B2014 have yielded compelling
504 predictions of plate motions, mantle flow, and plume drift that match many of the observations,
505 we caution that more work will be required to confirm a robust result. In many regards, the
506 geodynamic models so far have been simplistic; for example, B2014 models a constant viscosity
507 slab sinking in an isoviscous mantle, uses a limited subduction history as starting condition, and
508 must be extrapolated beyond its 72–42 Ma validity. Nevertheless, we believe further
509 consideration of geodynamic APM models is warranted, particularly those that address the
510 influence of mantle density heterogeneities and viscosity structures on plume drift and plate
511 motions. Such models need to be validated by all available data from geodesy, paleomagnetism,
512 and geochronology, and could further utilize additional constraints on mantle flow, such as
513 seismic anisotropy observations or seismic tomography models that reveal the tilts of plume
514 conduits or slabs in the deeper mantle. Likewise, more rigorous statistical treatment of trail
515 geometry, ages, and hotspot locations is needed to better quantify the uncertainties in the
516 resulting absolute plate and plume models.

517 518 **Acknowledgements**

519
520 We thank R. Gordon, T. Torsvik, B. Steinberger and an anonymous reviewer for comments that
521 greatly improved the manuscript. This work was partly supported by NSF grant OCE-1458964
522 (PW) and the Research Council of Norway through its Centres of Excellence funding scheme,
523 project number 223272 (CC). Original seamount age and paleolatitude data used in this study are
524 available from the cited references in Section 2 ((Tarduno, Duncan *et al.* 2003; Clouard and
525 Bonneville 2005; Kono, 1980; Koppers, Gowen *et al.* 2011; Koppers, Yamazaki *et al.* 2012;
526 Bono, Tarduno *et al.* 2019). This is SOEST contribution no. #####.

527 **References**

- 528
- 529 Acton, G.D. & Gordon, R.G., 1994. Paleomagnetic tests of Pacific plate reconstructions and
530 implications for motion between hotspots, *Science*, 263, 1246–1254.
- 531 Ballmer, M.D., Ito, G., Wolfe, C.J. & Solomon, S.C., 2013. Double layering of a
532 thermochemical plume in the upper mantle beneath Hawaii, *Earth Planet Sci Lett*, 376, 155–
533 164.
- 534 Barckhausen, U., Bagge, M. & Wilson, D.S., 2013. Seafloor spreading anomalies and crustal
535 ages of the Clarion-Clipperton Zone, *Mar. Geophys. Res.*, 34, 79–88.
- 536 Becker, T.W., Schaeffer, A.J., Lebedev, S. & Conrad, C.P., 2015. Toward a generalized plate
537 motion reference frame, *Geophysical Research Letters*, 42, 2015GL063695.
- 538 Bercovici, D., Ricard, Y. & Richards, M.A., 2000. The Relation Between Mantle Dynamics and
539 Plate Tectonics: A Primer. in *The History and Dynamics of Global Plate Motions*, pp. 5–46,
540 eds. Richards, M. A., Gordon, R. G. & van der Hilst, R. D. American Geophysical Union,
541 Washington, D.C.
- 542 Bono, R. K., J. A. Tarduno, and H. P. Bunge, 2019, Hotspot motion caused the Hawaiian-
543 Emperor Bend and LLSVPs are not fixed, *Nature Communications*, doi:10.1038/s41467-019-
544 11314-6.
- 545 Butterworth, N.P., Müller, R.D., Quevedo, L., O'Connor, J.M., Hoernle, K. & Morra, G., 2014.
546 Pacific plate slab pull and intraplate deformation in the early Cenozoic, *Solid Earth*, 5, 757–
547 777.
- 548 Chandler, M.T., Wessel, P., Taylor, B., Seton, M., Kim, S.-S. & Hyeong, K., 2012.
549 Reconstructing Ontong Java Nui: Implications for Pacific absolute plate motion, hotspot drift
550 and true polar wander, *Earth and Planetary Science Letters*, 331-332, 140–151.
- 551 Clague, D. A. , 1996, The growth and subsidence of the Hawaiian-Emperor volcanic chain, in
552 *The Origin and Evolution of Pacific Island Biotas*, edited by A. Keast and S. E. Miller, pp.
553 35–50, SPB Acad., Amsterdam.
- 554 Clouard, V., and A. Bonneville, 2005, Ages of seamounts, islands, and plateaus on the Pacific
555 plate, in *Plates, Plumes, and Paradigms*, edited by G. R. Foulger, J. H. Natland, D. C.
556 Presnall and D. L. Anderson, pp. 71–90, Geol. Soc. Am., Boulder, CO.
- 557 Conrad, C. P., and C. Lithgow-Bertelloni (2004), The temporal evolution of plate driving forces:
558 Importance of "slab suction" versus "slab pull" during the Cenozoic, *Journal of Geophysical*
559 *Research-Solid Earth*, 109(B10), doi:10.1029/2004jb002991.
- 560 Domeier, M., Shepard, G.E., Jakob, J., Gaina, C., Doubrovine, P.V. & Torsvik, T., 2017.
561 Intraoceanic subduction spanned the Pacific in the Late Cretaceous–Paleocene, *Science*
562 *Advances*, 3.
- 563 Doubrovine, P.V., Steinberger, B. & Torsvik, T.H., 2012. Absolute plate motions in a reference
564 frame defined by moving hot spots in the Pacific, Atlantic, and Indian oceans, *J. Geophys.*
565 *Res.*, 117, 10.1029/2011jb009072.
- 566 Duncan, R.A. & Clague, D.A., 1985. Pacific plate motion recorded by linear volcanic chains. in
567 *The Ocean Basins and Margins*, pp. 89–121, eds. Nairn, A. E. M., Stehli, F. G. & Uyeda, S.
568 Plenum, New York.
- 569 Faccenna, C., T. W. Becker, S. Lallemand, and B. Steinberger (2012), On the role of slab pull in
570 the Cenozoic motion of the Pacific plate, *Geophysical Research Letters*, 39,
571 doi:10.1029/2011gl050155.

- 572 Gordon, R. G., A. Cox, and C. E. Harter, 1978, Absolute motion of an individual plate estimated
573 from its ridge and trench boundaries, *Nature*, 274, 752–755.
- 574 Gordon, R.G., Late Cretaceous apparent polar wander of the Pacific plate: Evidence for a rapid
575 shift of the Pacific hotspots with respect to the spin axis, 1983, *Geophys. Res. Lett.*, 10, 709–
576 712.
- 577 Gordon, R. G., and C. D. Cape, 1981, Cenozoic latitudinal shift of the Hawaiian hotspot and its
578 implications for true polar wander, *Earth Planet. Sci. Lett.*, 55, 37–47.
- 579 Hassan, R., Müller, R.D., Gurnis, M., Williams, S.E. & Flament, N., 2016. A rapid burst in
580 hotspot motion through the interaction of tectonics and deep mantle flow, *Nature*, 533, 239–
581 242.
- 582 Koivisto, E.A., Andrews, D.L. & Gordon, R.G., 2014. Tests of fixity of the Indo-Atlantic hot
583 spots relative to Pacific hot spots, *Journal of Geophysical Research: Solid Earth*, 119, 661–
584 675.
- 585 Kono, M., 1980, Paleomagnetism of DSDP Leg 55 basalts and implications for the tectonics of
586 the Pacific plate, in *Init. Reports. DSDP*, edited by E. D. Jackson, et al., pp. 737–752, US
587 Govt. Printing Office, Washington.
- 588 Konrad, K., Koppers, A.A., Steinberger, B., Finlayson, V.A., Konter, J. & Jackson, M.G., 2018.
589 On the relative motions of long-lived Pacific mantle plumes, *Nature Communications*, 9, 1–8.
- 590 Koppers, A.A.P., Duncan, R.A. & Steinberger, B., 2004. Implications of a nonlinear $^{40}\text{Ar}/^{39}\text{Ar}$
591 age progression along the Louisville seamount trail for models of fixed and moving hot spots,
592 *Geochemistry, Geophysics, Geosystems*, 5, doi:10.1029/2003GC000671.
- 593 Koppers, A.A.P., Gowen, M.D., Colwell, L.E., Gee, J.S., Lonsdale, P.F., Mahoney, J.J. &
594 Duncan, R.A., 2011. New $^{40}\text{Ar}/^{39}\text{Ar}$ age progression for the Louisville hot spot trail and
595 implications for inter-hot spot motion, *Geochem. Geophys. Geosyst.*, 12,
596 doi:10.1029/2011GC003804.
- 597 Koppers, A.A.P., Phipps Morgan, J., Morgan, J.W. & Staudigel, H., 2001. Testing the fixed
598 hotspot hypothesis using $^{40}\text{Ar}/^{39}\text{Ar}$ age progressions along seamount trails, *Earth Planet. Sci.*
599 *Lett.*, 185, 237–252.
- 600 Koppers, A.A.P., Yamazaki, T., Geldmacher, J., Gee, J.S., Pressling, N., Hoshi, H., Anderson, L.,
601 Beier, C., Buchs, D.M., Chen, L.H., Cohen, B.E., Deschamps, F., Dorais, M.J., Ebuna, D.,
602 Ehmann, S., Fitton, J.G., Fulton, P.M., Ganbat, E., Hamelin, C., Hanyu, T., Kalnins, L., Kell,
603 J., Machida, S., Mahoney, J.J., Moriya, K., Nichols, A.R.L., Rausch, S., Sano, S.i., Sylvan,
604 J.B. & Williams, R., 2012. Limited latitudinal mantle plume motion for the Louisville
605 hotspot, *Nature Geosci*, 5, 911–917.
- 606 Le Pichon, X., 1968. Sea floor spreading and continental drift, *J. Geophys. Res.*, 73, 3661–3697.
- 607 Maher, S.M., Wessel, P., Müller, R.D., Williams, S.E. & Harada, Y., 2015. Absolute plate
608 motion of Africa around Hawaii-Emperor bend time, *Geophys. J. Int.*, 201, 1743–1764.
- 609 McKenzie, D.P. & Parker, R.L., 1967. The North Pacific: an example of tectonics on a sphere,
610 *Nature*, 216, 1276–1280.
- 611 Mishra, J.K. & Gordon, R.G., 2016. The rigid-plate and shrinking-plate hypotheses: Implications
612 for the azimuths of transform faults, *Tectonics*, 35, 1827–1842.
- 613 Morgan, W.J., 1968. Rises, trenches, great faults and crustal blocks, *J. Geophys. Res.*, 73, 1959–
614 1982.
- 615 Morgan, W.J., 1971. Convection plumes in the lower mantle, *Nature*, 230, 43–44.
- 616 Morgan, J. W., 1981, Hotspot tracks and the opening of the Atlantic and Indian oceans, in *The*
617 *sea*, edited by C. Emiliani, Wiley, New York.

- 618 Müller, R.D., Seton, M., Zahirovic, S., Williams, S.E., Matthews, K.J., Wright, N.M., Shephard,
619 G.E., Maloney, K.T., Barnett-Moore, N., Hosseinpour, M., Bower, D.J. & Cannon, J., 2016.
620 Ocean basin evolution and global-scale plate reorganization events since Pangea breakup,
621 *Ann. Rev. Earth Planet. Sci.*, 44, 107–138.
- 622 O'Connor, J.M., Steinberger, B., Regelous, M., Koppers, A.A., Wijbrans, J.R., Haase, K.M.,
623 Stoffers, P., Jokat, W. & Garbe-Schonberg, D., 2013. Constraints on past plate and mantle
624 motion from new ages for the Hawaiian-Emperor Seamount Chain, *Geochem. Geophys.*
625 *Geosyst.*, 14, 4564–4584.
- 626 O'Neill, C., Müller, D. & Steinberger, B., 2005. On the uncertainties in hot spot reconstructions
627 and the significance of moving hot spot reference frames, *Geochem. Geophys. Geosyst.*, 6,
628 doi:10.1029/2004GC000784.
- 629 Petronotis, K. E., R. G. Gordon, and G. D. Acton, 1994, A 57 Ma Pacific paleomagnetic pole
630 determined from a skewness analysis of crossings of marine magnetic anomaly 25r, *Geophys.*
631 *J. Int.*, 118, 529–554.
- 632 Raymond, C.A., Stock, J.M. & Cande, S.E., 2000. Fast Paleogene motion of the Pacific hotspots
633 from revised global plate circuit constraints. in *The history and dynamics of global plate*
634 *motions*, pp. 359–375, eds. Richards, M. A., Gordon, R. G. & van der Hilst, R. D. AGU,
635 Washington, DC.
- 636 Richards, M.A. & Lithgow-Bertelloni, C., 1996. Plate motion changes, the Hawaiian-Emperor
637 bend, and the apparent success and failure of geodynamic models, *Earth and Planetary*
638 *Science Letters*, 137, 19-27.
- 639 Sharp, W.D. & Clague, D.A., 2006. 50-Ma initiation of Hawaii-Emperor bend records major
640 change in Pacific plate motion, *Science*, 313, 1281–1284.
- 641 Steinberger, B., 2000. Plumes in a convecting mantle: models and observations for individual
642 hotspots, *J. Geophys. Res.*, 05, 11,127–111,152.
- 643 Steinberger, B. & O'Connell, R.J., 1998. Advection of plumes in mantle flow: Implications for
644 hot spot motion, mantle viscosity and plume distributions, *Geophys. J. Int.*, 132, 412–434.
- 645 Steinberger, B. & Gaina, C., 2007. Plate tectonic reconstructions predict part of Hawaiian
646 hotspot track to be preserved in Bering Sea, *Geology*, 35, 407-410.
- 647 Steinberger, B., Sutherland, R. & O'Connell, R.J., 2004. Prediction of Emperor-Hawaii seamount
648 locations from a revised model of global plate motion and mantle flow, *Nature*, 430, 167–
649 173.
- 650 Tarduno, J. A., and R. D. Cottrell, 1997, Paleomagnetic evidence for motion of the Hawaiian
651 hotspot during formation of the Emperor seamounts, *Earth Planet. Sci. Lett.*, 153(3-4), 171–
652 180.
- 653 Tarduno, J. A., et al., 2003, The Emperor Seamounts: Southward Motion of the Hawaiian
654 Hotspot Plume in Earth's Mantle, *Science*, 301(5636), 1064–1069.
- 655 Tarduno, J.A., Bunge, H.-P., Sleep, N.H. & Hansen, U., 2009. The Bent Hawaiian-Emperor
656 Hotspot Track: Inheriting the Mantle Wind, *Science*, 324, 50–53.
- 657 Torsvik, T., R. D. Müller, R. Van der Voo, B. Steinberger, and C. Gaina, 2008, Global Plate
658 Motion Frames: Toward a unified model, *Rev. Geophys.*, 46(RG3004),
659 doi:10.1029/2007RG000227.
- 660 Torsvik, T., Doubrovine, P.V., Steinberger, B., Gaina, C., Spakman, W. & Domeier, M., 2017.
661 Pacific plate motion change caused the Hawaiian-Emperor Bend, *Nature Communications*, 8.
- 662 Wang, C., R. G. Gordon, T. Zhang, and L. Zheng, 2019, Observational Test of the Global
663 Moving Hot Spot Reference Frame, *Geophys. Res. Lett.*, 46(14), 8031-8038.

- 664 Wang, C., R. G. Gordon, and T. Zhang, 2017, Bounds on geologically current rates of motion of
665 groups of hot spots, *Geophys. Res. Lett.*, *44*, 6048–6056.
- 666 Wessel, P. & Conrad, C.P., 2017. Assessing Pacific Absolute Plate and Plume Motions,
667 *Geological Society of America Abstracts with Programs*, *49*, Abstract 10.11.
- 668 Wessel, P. & Kroenke, L.W., 2008. Pacific absolute plate motions since 145 Ma: An assessment
669 of the fixed hotspot hypothesis, *J. Geophys. Res.*, *113*, doi:10.1029/2007JB005499.
- 670 Wessel, P. & Kroenke, L.W., 2009. Observations of geometry and ages constrain relative motion
671 of Hawaii and Louisville plumes, *Earth Planet. Sci. Lett.*, *284*, 467–472.
- 672 Wessel, P. & Müller, R.D., 2016. Ridge-spotting: A new test for Pacific absolute plate motion
673 models, *Geochem. Geophys. Geosyst.*, *17*, 2408–2420.
- 674 Wilson, D.S., 2016. Revision of Paleogene plate motions in the Pacific and implications for the
675 Hawaiian-Emperor bend: Comment, *Geology Forum*, e384.
- 676 Wilson, J.T., 1963. A possible origin of the Hawaiian Islands, *Can. J. Phys.*, *41*, 863–870.
- 677 Woodworth, D., Gordon, R.G., Seidman, L. & Zheng, L., 2017. True Polar Wander and the
678 Origin of the Hawaiian-Emperor Bend: New Evidence, *AGU Fall Meeting Abstracts*,
679 GP51A-0781.
- 680 Woodworth, D. & Gordon, R. G., 2018, Paleolatitude of the Hawaiian hot spot since 48 Ma:
681 Evidence for a mid-Cenozoic true polar stillstand followed by late Cenozoic true polar
682 wander coincident with Northern Hemisphere glaciation. *Geophys. Res. Lett.*, *45*, 11,632-
683 11,640, doi:10.1029/2018GL080787.
- 684

685 **Figure Captions**

686
 687 **Figure 1.** a) Location map showing the Hawaii (HI) and Louisville (LV) chains, with sub-
 688 regions studied (rectangles). b) Bathymetry of the Emperor chain, showing empirical central line
 689 (orange) with available samples (red triangles) and their ages in Myr. HEB indicates the ~Chron
 690 21o bend with yellow uncertainty ellipse on the bend location. c) Bathymetry of the older
 691 Louisville chain, similarly showing empirical central line (orange), available samples (red
 692 triangles) and their ages in Myr. LVB indicates the ~Chron 21o bend with yellow uncertainty
 693 ellipse. Gray labels indicate inferred paleolatitudes, λ , from paleomagnetism.

694
 695 **Figure 2.** Observed sample ages (red circles) for the Hawaii-Emperor and Louisville chains,
 696 plotted versus the distance along each chain's empirical central line. Light blue envelope
 697 contains all observed ages (except one known outlier for HI and larger variability for LV in the
 698 40–60 Ma range). See text for discussion and supplementary material for data sets.
 699

700 **Figure 3.** Eight proposed models for Pacific absolute motion (see text). Rainbow-colored paths
 701 reflect predictions of past motion of points presently at the two hotspots; these paths only
 702 coincide with the two hotspot trails for fixed-hotspot models. Hot-cold paths reflect the
 703 published plume drift histories for D2012 and H2016; see text for discussion.
 704

705 **Figure 4.** Inferred Hawaii plume paths for the 8 APM models obtained by reconstructing the
 706 smooth, continuous age progressions back to zero age, with the explicit paths for D2012 and
 707 H2016 as thick colored lines. The color of these paths reflects the age (in Ma; bottom right). The
 708 colored triangles represent reconstructed individual samples, while colored circles represent
 709 misfits between observed and predicted paleolatitudes, $\Delta\lambda$, as coded by the colors shown on the
 710 top right (magenta colors mean underpredicted, orange colors mean overpredicted).
 711

712 **Figure 5.** Same as Fig. 4 but for Louisville plume paths. Black dotted line in panels for OMS05
 713 and M2015C is the prediction for B2014, for first-order comparison.
 714

715 **Figure 6.** Predicted Hawaii (a) and Louisville (b) trails (color-coded circles, color table A) and
 716 plume paths (colored path, color table B) for B2014 (larger circles) and D2012 (smaller circles).
 717 The colored triangles represent observed seamount samples. Squares on plume paths are
 718 predicted paleolatitudes, with right-side map annotations indicating observed paleolatitude
 719 ranges.
 720

721 **Figure 7.** Implicit mean hotspot drift rates before and after HEB, as implied by published APM
 722 models (see legend for models). Gray band reflect the 51–47 Ma time window of HEB formation.
 723 a) Hawaii plume drift rates. B) Louisville plume drift rates. D2012* refers to the explicit model.
 724 Note that WK08A is identical to, and plotted behind, WK08D after the HEB. Gray hachured area
 725 shows a limit on inter-hotspot motion (Koivisto et al., 2014) since 48 Ma and gray dashed line
 726 gives an upper limit on recent hotspot motion (last 10 Ma; Wang et al., 2019).
 727

728 **Figure 8.** Inferred Pacific absolute plate speed as implied by published APM models (see legend
 729 for models). Gray band reflects the 51–47 Ma time window of HEB formation. a) Plate speeds at

730 Hawaii hotspot. B) Plate speeds at Louisville hotspot. The dashed part of B2014 indicates where
731 we extended the model (extension of oldest stage back to 80 Ma and following WK08D after 42
732 Ma). Green triangles indicate current plate speed from HS4-UW-MORVEL56 (Wang et al.,
733 2017).

734
735 **Figure 9.** Longitude and latitude of plume drift versus time; see legend for APM models. Gray
736 horizontal band indicates the 51–47 Ma time window of HEB formation. Gray symbols with
737 error bars represent observed paleolatitudes with $\pm 2\sigma$ uncertainties.

738
739 **Figure 10.** Grouping of APM model results for Hawaii (red) and Louisville (blue) in terms of the
740 misfit to paleolatitude observations versus the pre-bend/post-bend drift rate ratios. Ellipses
741 highlight the D2012 implicit and explicit (marked by asterisk) results versus the B2014 implicit
742 results.

743
744

Figure 1.

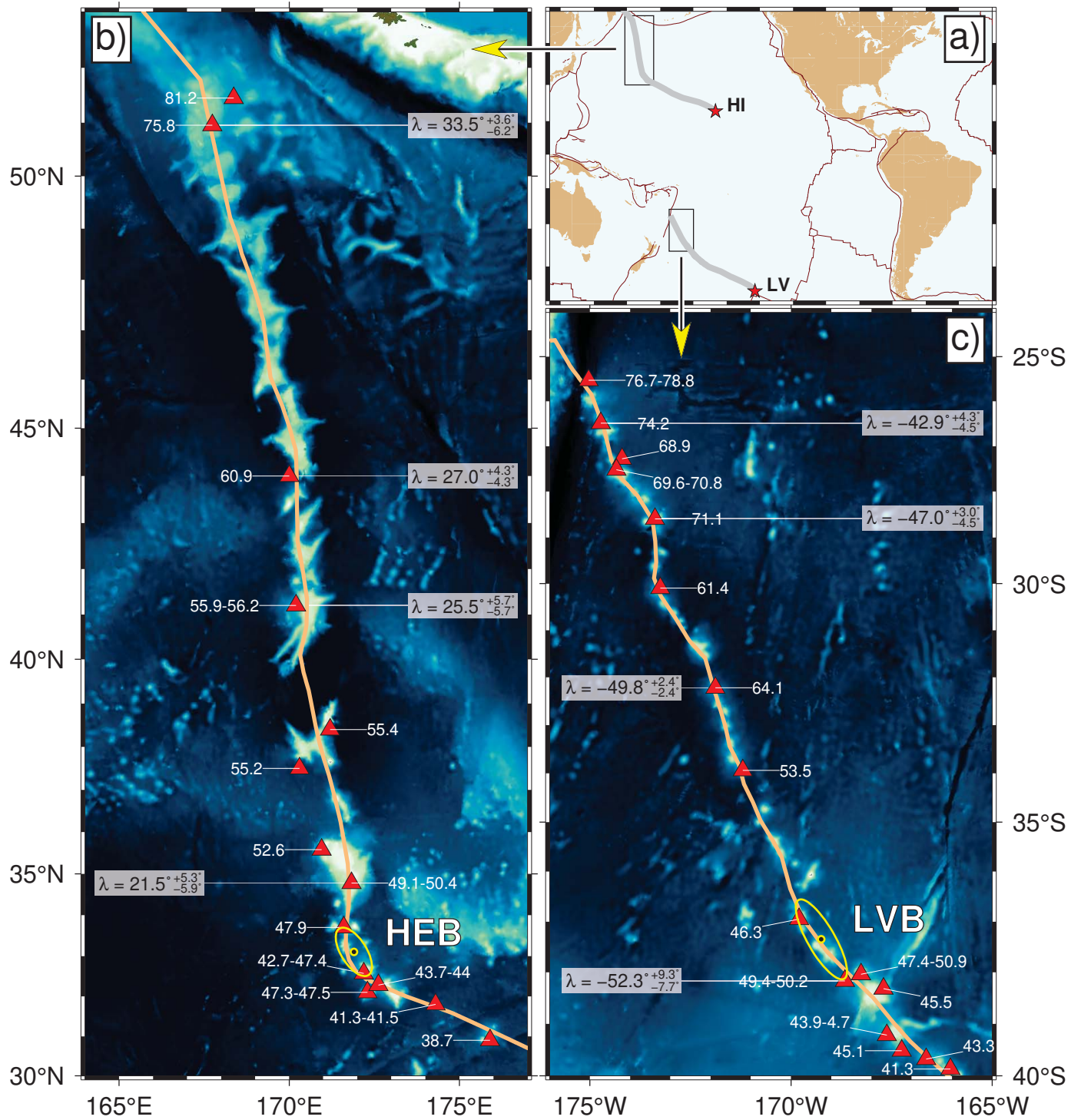


Figure 2.

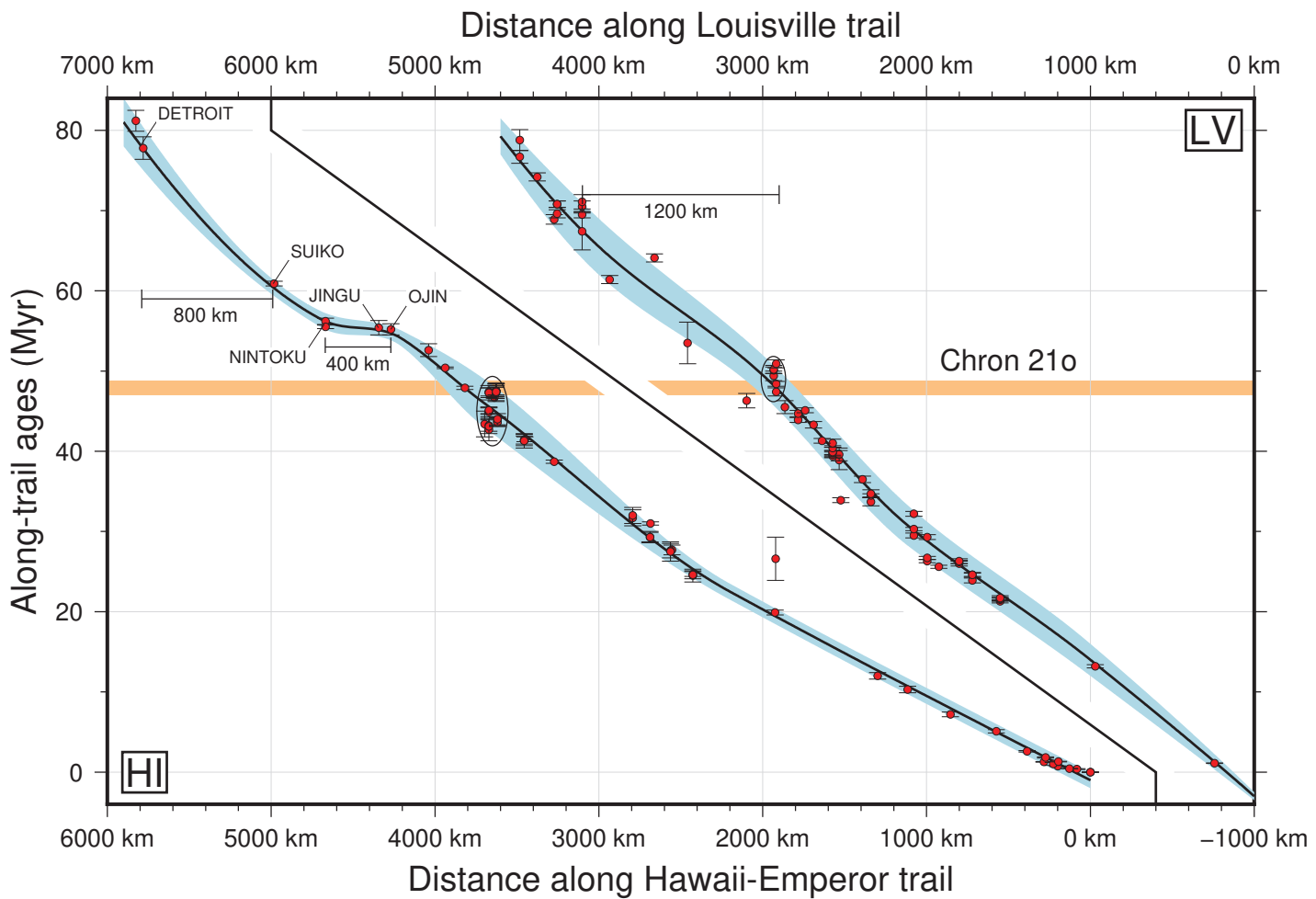


Figure 3.

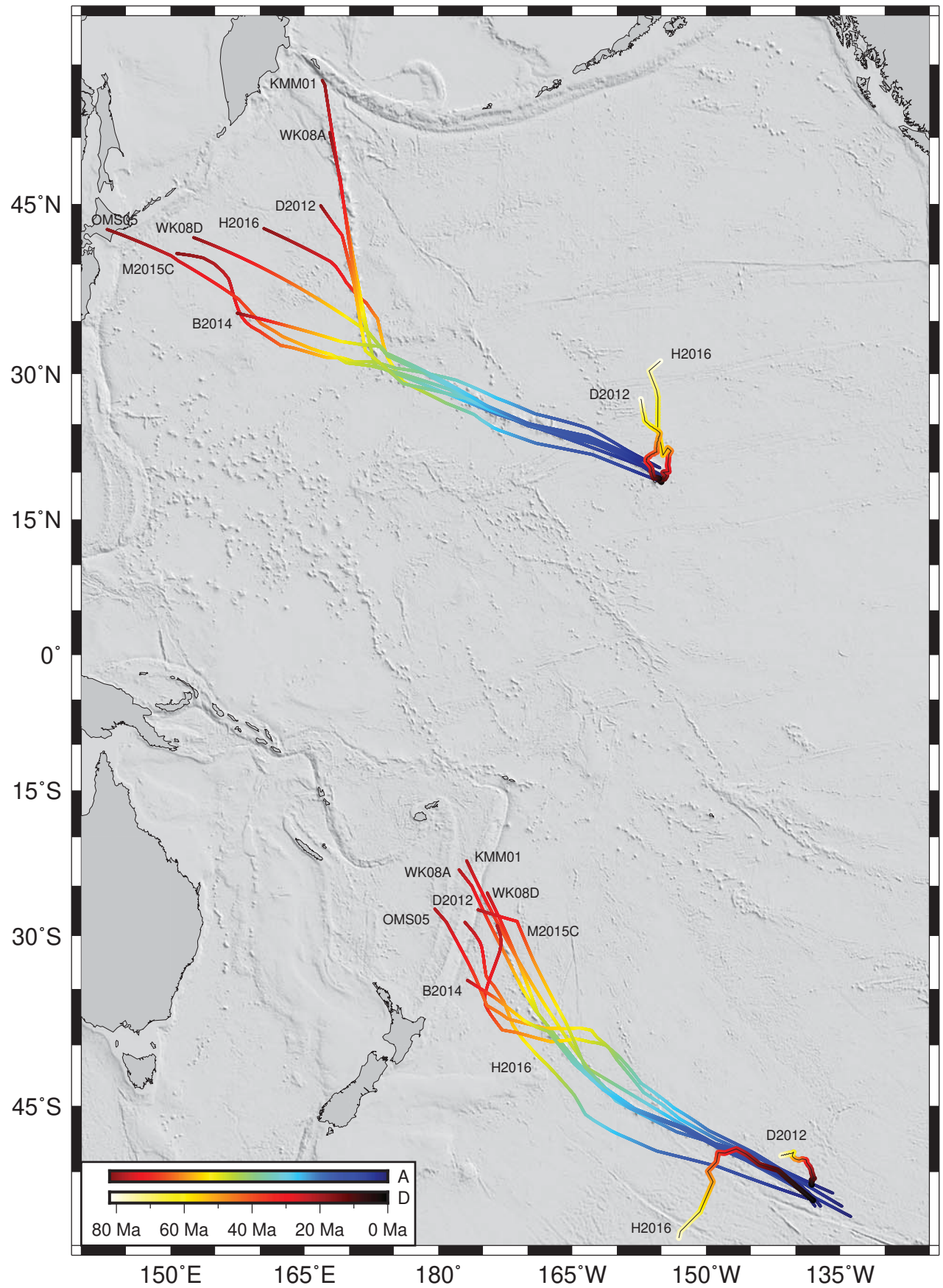


Figure 4.

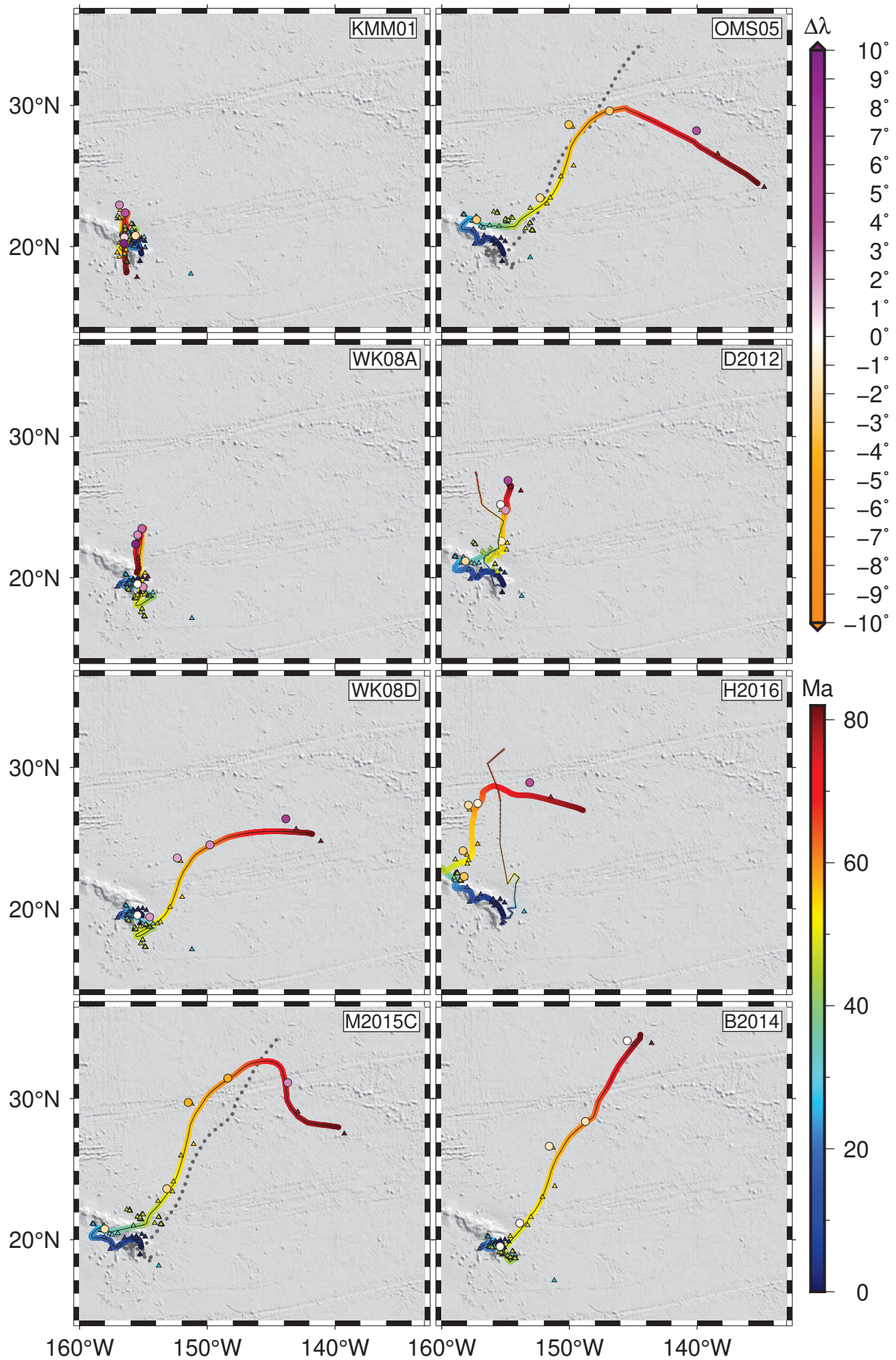


Figure 5.

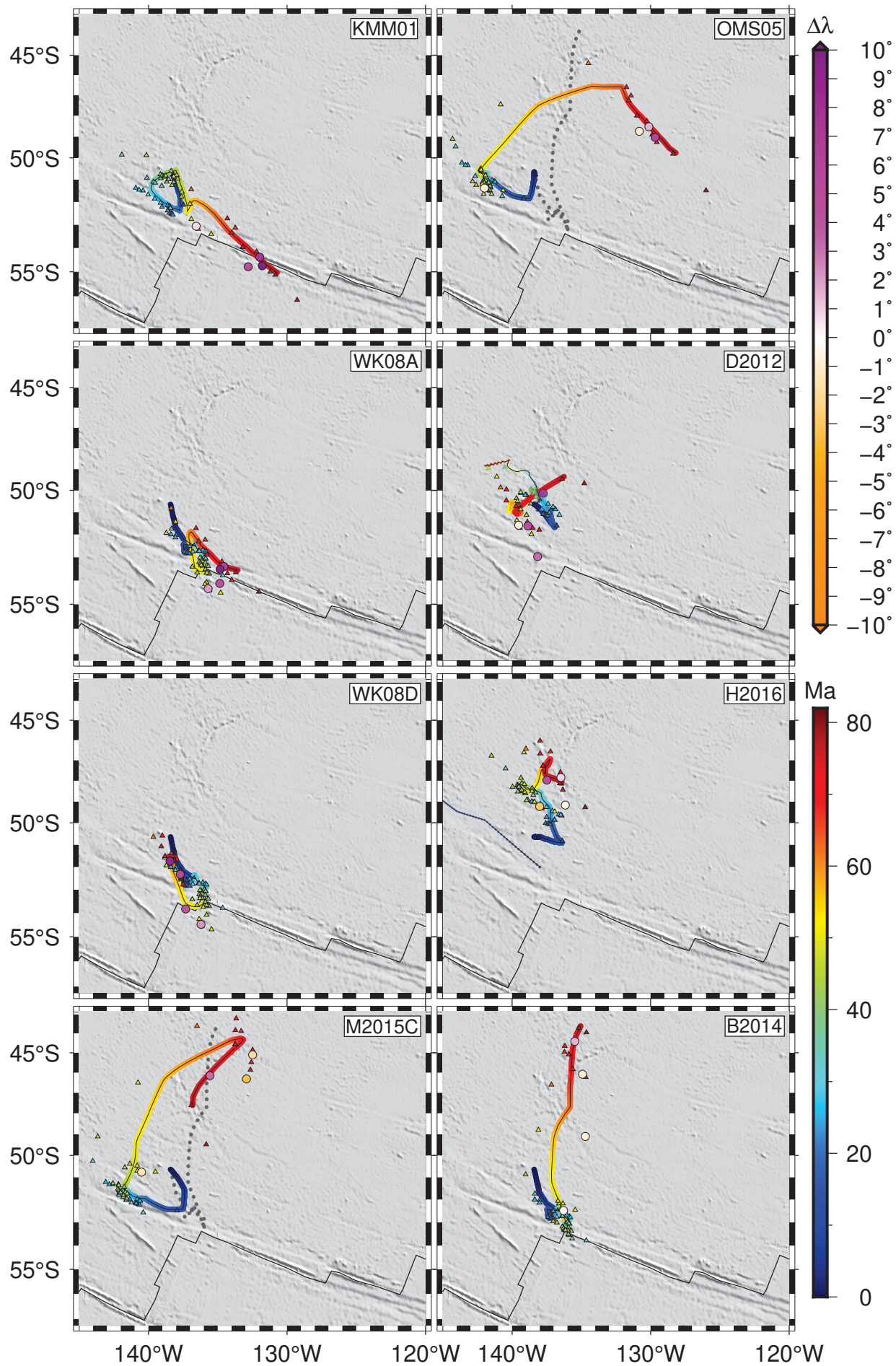


Figure 6.

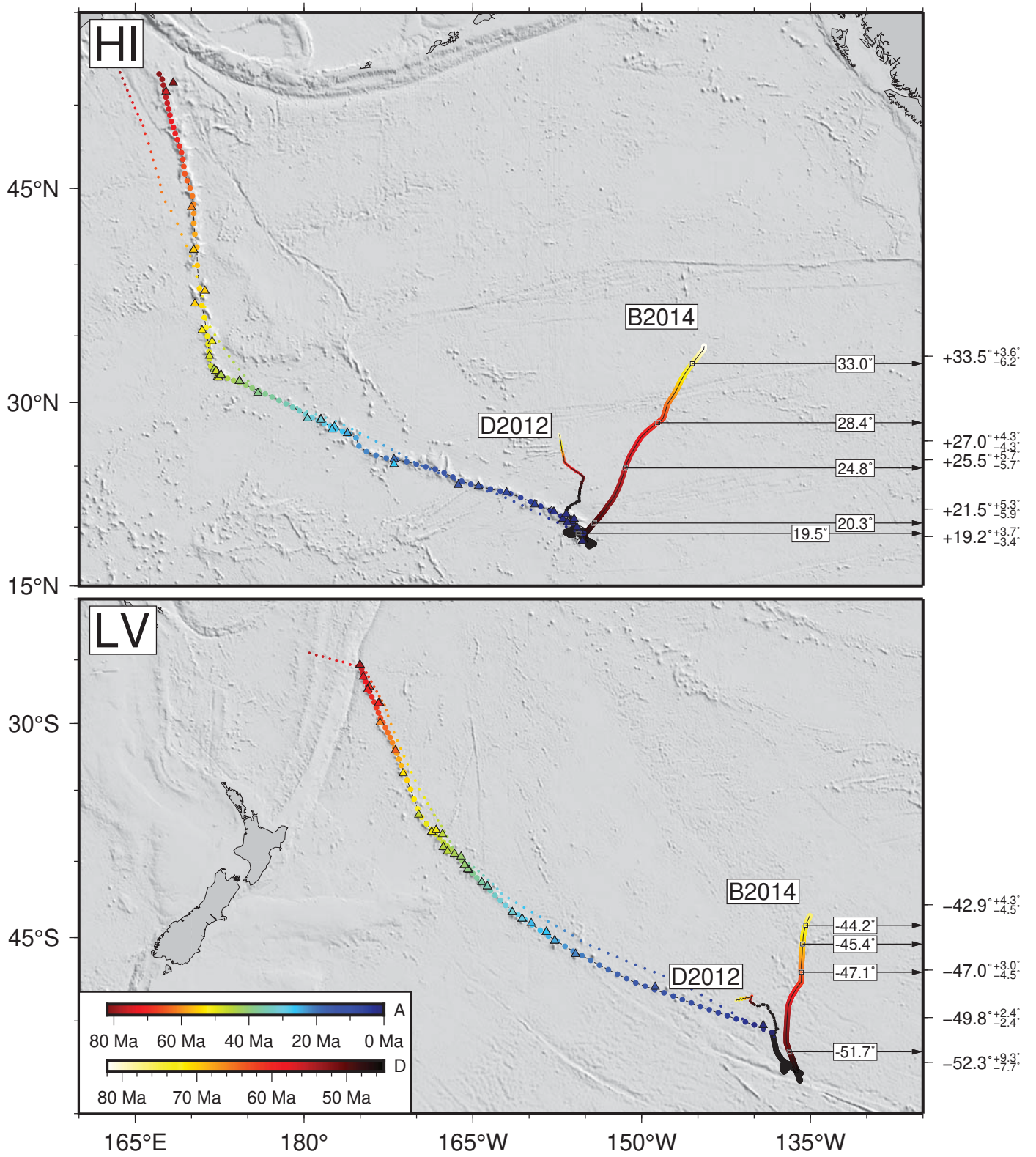


Figure 7.

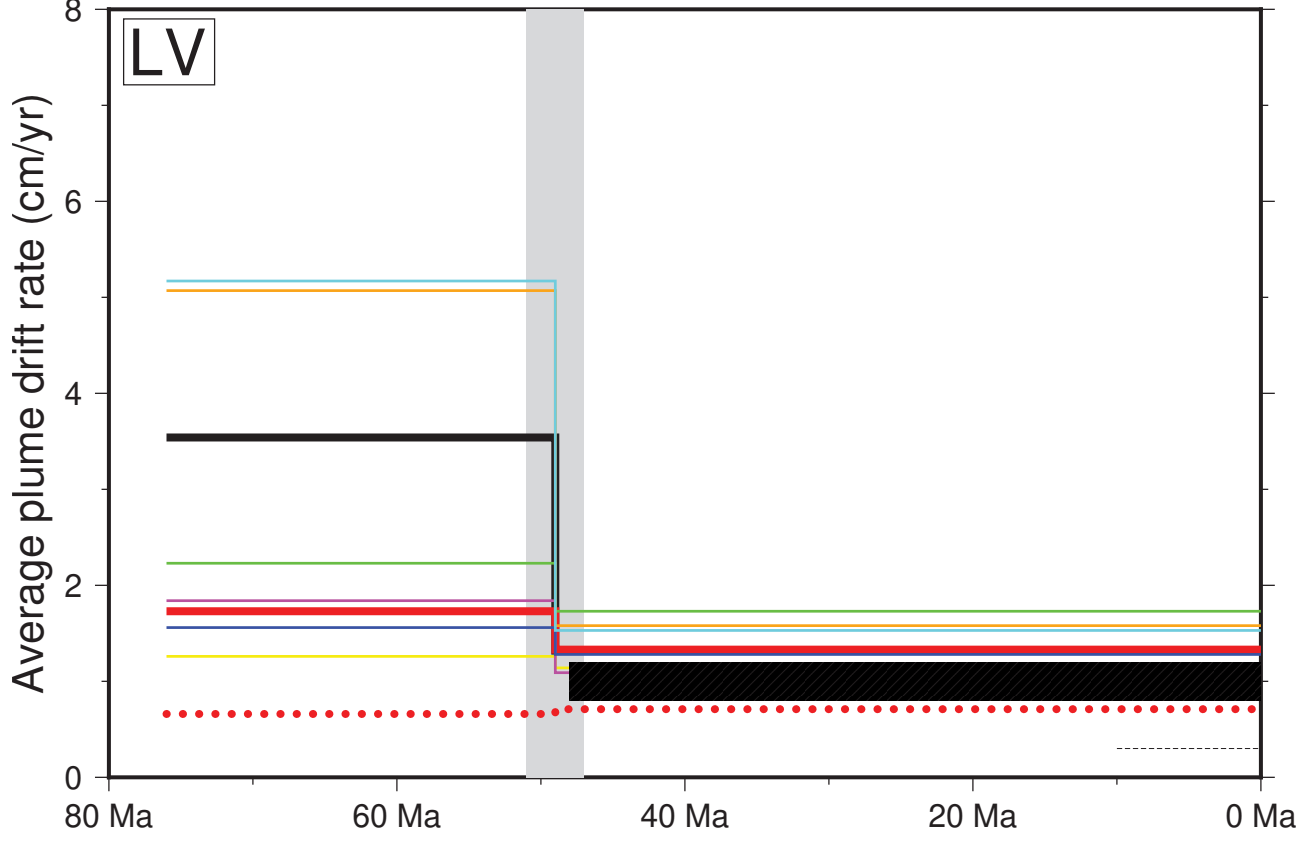
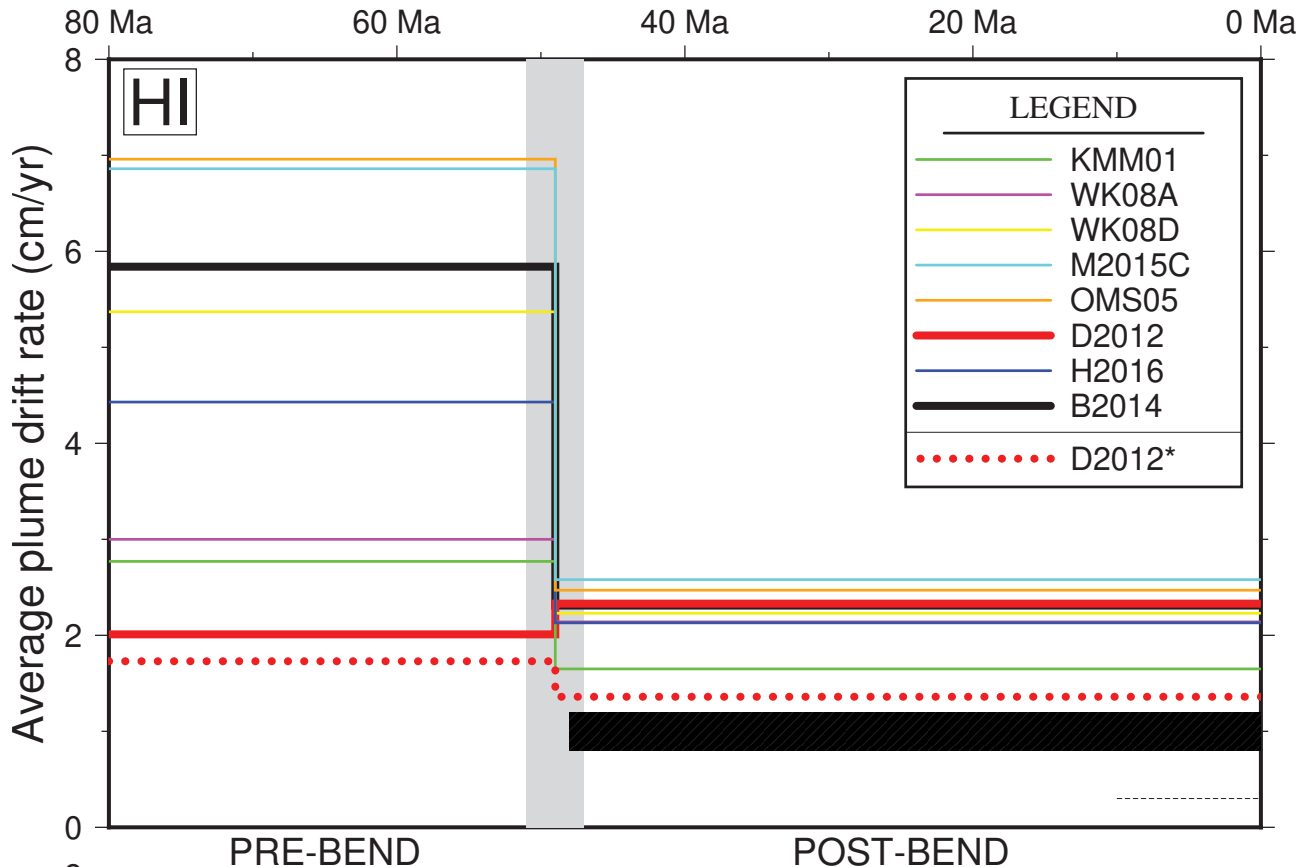


Figure 8.

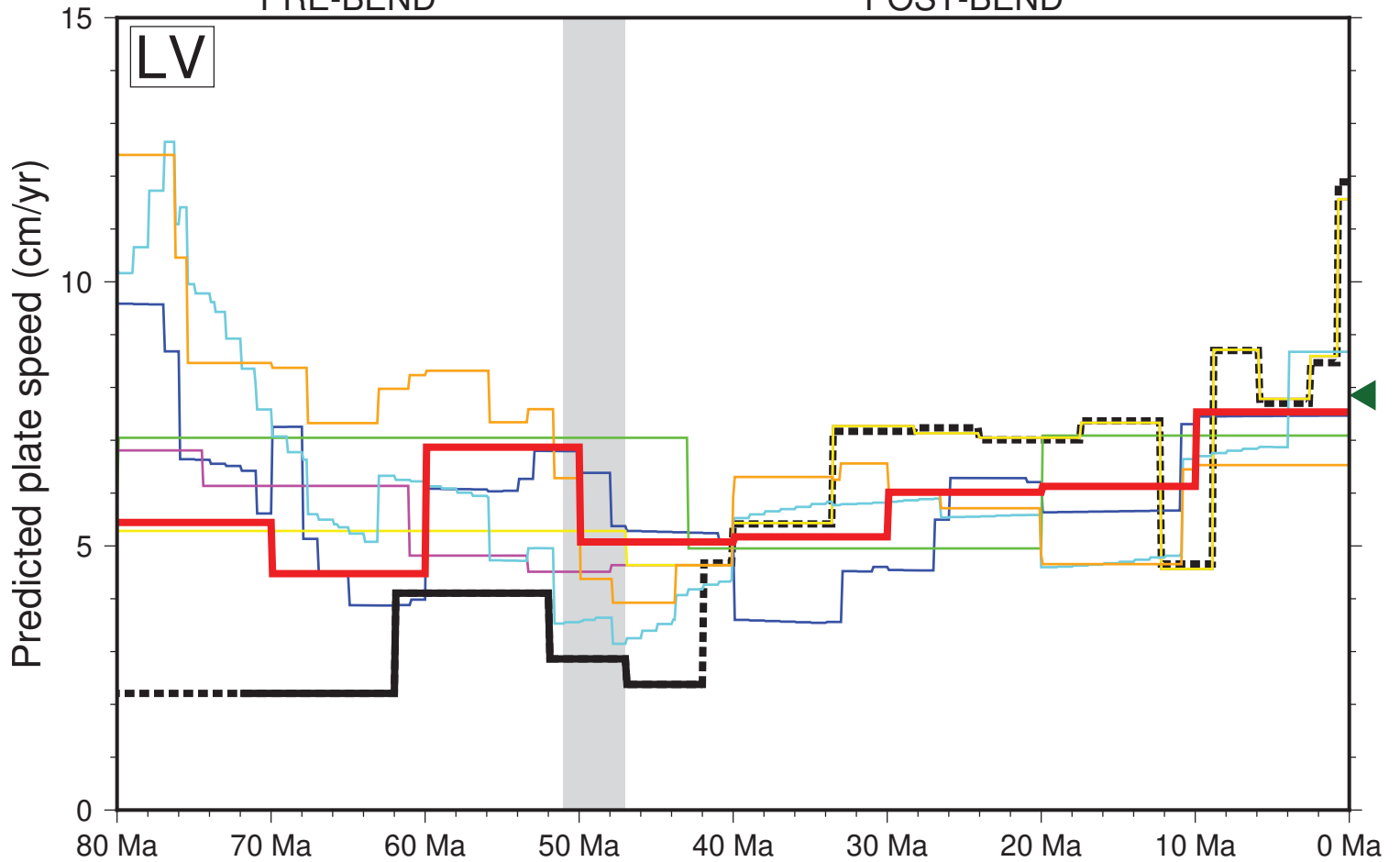
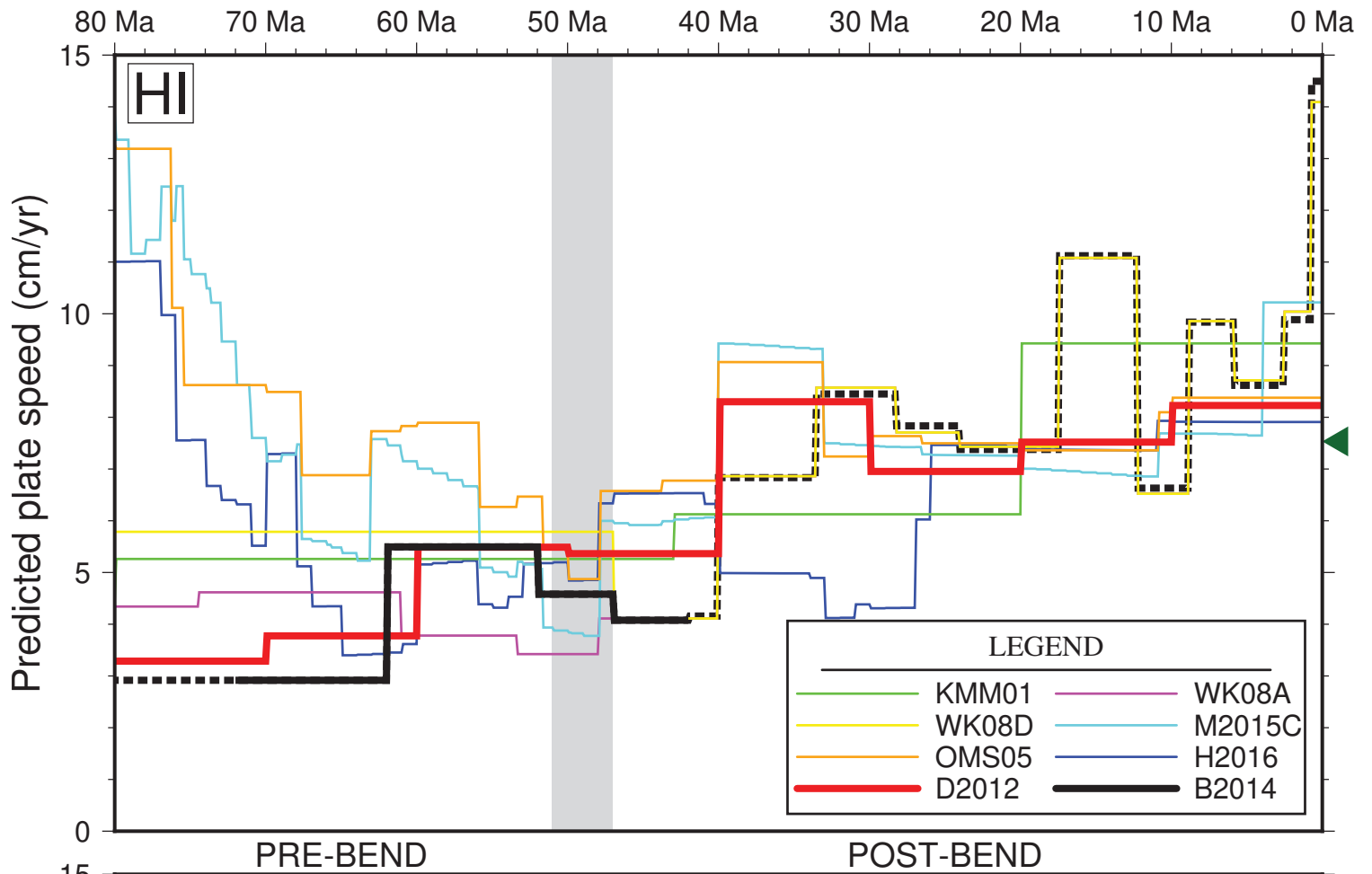


Figure 9.

Longitude

Latitude

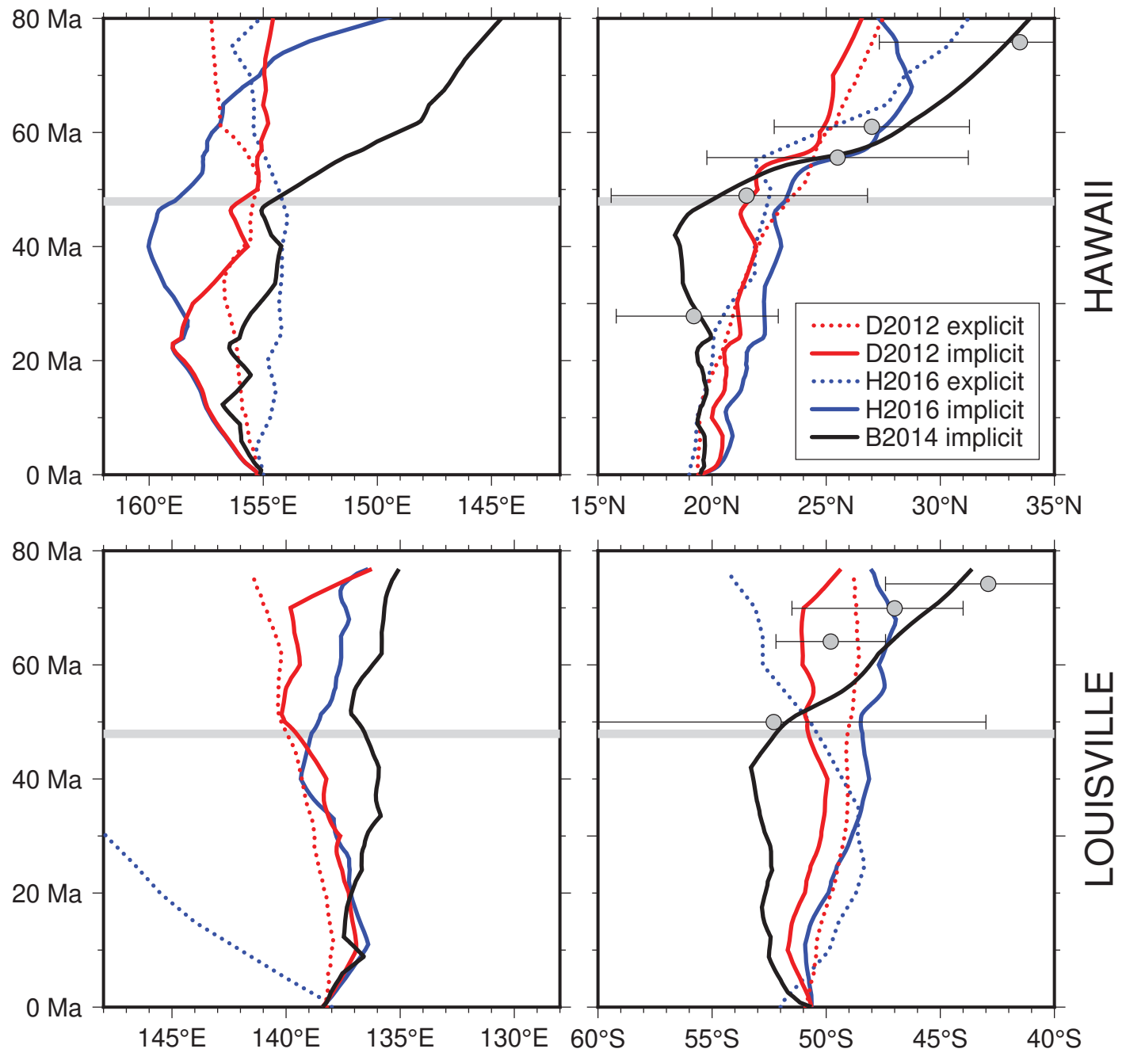


Figure 10.

